GA–A26875

OPTIMIZATION OF THE SAFETY FACTOR PROFILE FOR HIGH NONINDUCTIVE CURRENT FRACTION DISCHARGES IN DIII-D

by
J.R. FERRON, C.T. HOLCOMB, T.C. LUCE, P.A. POLITZER, F. TURCO, A.E. WHITE, J.C. DeBOO, E.J. DOYLE, A.W. HYATT, R.J. LA HAYE, M. MURAKAMI, T.W. PETRIE, C.C. PETTY, T.L. RHODES, and L. ZENG

AUGUST 2010

GENERAL ATOMICS

DISCLAIMER

GA–A26875

OPTIMIZATION OF THE SAFETY FACTOR PROFILE FOR HIGH NONINDUCTIVE CURRENT FRACTION DISCHARGES IN DIII-D

by
J.R. FERRON, C.T. HOLCOMB,* T.C. LUCE, P.A. POLITZER, F. TURCO,† A.E. WHITE,‡ J.C. DeBOO, E.J. DOYLE,¶ A.W. HYATT, R.J. LA HAYE, M. MURAKAMI§, T.W. PETRIE, C.C. PETTY, T.L. RHODES,¶ and L. ZENG¶

This is a preprint of a paper to be presented at the 23rd IAEA Fusion Energy Conference, October 11–16, 2010 in Daejon, Republic of Korea and to be published in Proceedings.

*Lawrence Livermore National Laboratory, Livermore, California
†Oak Ridge Institute of Science and Education, Oak Ridge, Tennessee
‡Massachusetts Institute of Technology, Cambridge, Massachusetts
¶University of California-Los Angeles, Los Angeles, California
§Oak Ridge National Laboratory, Oak Ridge, Tennessee

Work supported in part by
the U.S. Department of Energy
under DE-FC02-04ER54698, DE-AC52-07NA27348, DE-AC05-06OR23100, DE-FC02-93ER54186, DE-FG03-08ER54984, and DE-AC05-00OR22725

GENERAL ATOMICS PROJECT 30200
AUGUST 2010

GENERAL ATOMICS

Optimization of the Safety Factor Profile for High Noninductive Current Fraction Discharges in DIII-D

J.R. Ferron[1], C.T. Holcomb[2], T.C. Luce[1], P.A. Politzer[1], F. Turco[3], A.E. White[4], J.C. DeBoo[1], E.J. Doyle[5], A.W. Hyatt[1], R.J. La Haye[1], M. Murakami[6], T.W. Petrie[1], C.C. Petty[1], T.L. Rhodes[5], and L. Zeng[5]

[1]General Atomics, P.O. Box 85608, San Diego, California 92186-5608
[2]Lawrence Livermore National Laboratory, Livermore, California
[3]Oak Ridge Institute for Science Education, Oak Ridge, Tennessee
[4]Massachusetts Institute of Technology, Cambridge, Massachusetts
[5]University of California-Los Angeles, Los Angeles, California
[6]Oak Ridge National Laboratory, Oak Ridge, Tennessee

e-mail contact of main author: ferron@fusion.gat.com

Abstract. In order to assess the optimum q profile for discharges in DIII-D with 100% of the current driven noninductively (f_{NI} = 1), the self-consistent response of the plasma profiles to changes in the q profile was studied in high f_{NI}, high β_N discharges through a scan of q_{min} and q_{95} at two values of β_N. As expected, both the bootstrap current fraction, f_{BS}, and f_{NI} increased with q_{95}. The temperature and density profiles were found to broaden as either q_{min} or β_N is increased. A consequence is that f_{BS} does not continue to increase at the highest values of q_{min}. A scaling function that depends on q_{min}, q_{95}, and the peaking factor for the thermal pressure was found to represent well the f_{BS}/β_N inferred from the experimental profiles. The changes in the shapes of the density and temperature profiles as β_N is increased modify the bootstrap current density (J_{BS}) profile from peaked close to the axis to relatively flat in the region between the axis and the H-mode pedestal. Therefore, significant externally driven current density in the region inside the H-mode pedestal is required in addition to J_{BS} in order to match the profiles of the noninductive current density (J_{NI}) to the desired total current density (J). In this experiment, the additional current density was provided mostly by neutral beam current drive. The profiles of J_{NI} and J were most similar at $q_{min} \approx 1.35$-1.65, $q_{95} \approx 6.8$, where f_{BS} is also maximum, establishing this q profile as the optimal choice for f_{NI} = 1 operation in DIII-D with the existing set of external current drive sources.

1. Introduction

In a tokamak discharge with 100% noninductively driven current (f_{NI} = 1) and a large fraction of self-generated bootstrap current [1] (f_{BS}), the safety factor (q) profile plays a key role as a result of the close coupling to both the transport coefficients and the sources of noninductive current density [2]. The bootstrap current density (J_{BS}) is proportional to the local values of q and the temperature and density gradients, but the q profile is strongly dependent on J_{BS} when f_{BS} is large. In a steady-state tokamak, f_{BS} will be as large as possible in order to minimize the required external current drive power [3]. The temperature and density gradients depend on the transport coefficients, which also depend on q as well as the magnetic shear. The stability limits to increasing pressure depend on the q profile and the gradients. Finally, the amount of current that can be driven by external sources depends on the temperature and density profiles [3]. The complexity of these interactions and of the underlying processes limits the present ability to predict the self-consistent density, temperature, and q profiles using models.

In order to assess the optimum q profile for f_{NI} = 1 discharges in DIII-D, the self-consistent response of the plasma profiles to changes in the q profile was studied in high f_{NI}, high normalized toroidal β (β_N) discharges. In a systematic scan of the minimum value of q ($1 < q_{min} < 2$) and q at 95% of the normalized flux ($4.5 < q_{95} < 6.8$), the temperature and density profiles were measured and the inferred profiles of the noninductively driven current densities (bootstrap, neutral beam driven J_{NBCD}, electron cyclotron driven J_{ECCD}) and the noninductive current fractions were computed from models. Measurements were made at both $\beta_N \approx 2.8$ and at the β_N achieved with the maximum available neutral beam heating power, β_N = 3.1 to 3.8.

As expected, both f_{BS} and f_{NI} increased with q_{95}. However, the temperature and density profiles were found to broaden as either q_{min} or β_N is increased. Because of these profile changes and the role of q_{min} in determining the total bootstrap driven current, the relation [3]

$$f_{BS} \propto \varepsilon^{0.5} \beta_P \propto q_{95} \beta_N \quad (1)$$

is not the best description of the results in these experiments. An alternative scaling function is presented here that depends on q_{min} and a measure of the pressure profile peaking in addition to q_{95} and β_N. As β_N was increased, the changes in the shapes of the density and temperature profiles were found to modify the J_{BS} profile from peaked close to the axis to relatively flat in the region between the axis and the H-mode pedestal. A peaked noninductive current density (J_{NI}) profile is required, however, to match the total current density (J). Therefore, significant externally driven current density in the region inside the H-mode pedestal is required in addition to J_{BS} to match the profiles of J_{NI} and the desired total J. These profiles were most similar at $q_{min} \approx 1.35$-1.65, $q_{95} \approx 6.8$, where f_{BS} is also maximum, establishing this q profile as the optimum choice for $f_{NI} = 1$ operation in DIII-D with the existing set of external current drive sources.

2. Description of the Experiment

The discharges for this experiment were created using the approach previously found to be optimum for high noninductive current fraction experiments in DIII-D [4]. Neutral beams at total power up to 13.5 MW from 5 beam sources that inject in the direction of the plasma current were the primary external power source, with additional heating from gyrotron power (up to 3.2 MW) applied as electron cyclotron current drive deposited in the region $0.25 < \hat{\rho} < 0.6$. ($\hat{\rho} = \rho/\rho_b$ is the normalized plasma radius, where ρ is the square root of the normalized toroidal magnetic flux and ρ_b is its value at the discharge boundary.) The q profile was varied by changing the values of q_{95} and q_{min}. The preprogrammed timing of the H-mode transition and the time evolution of β_N were varied during the discharge formation in order to change the value of q_{min} during the plasma current flattop. Data are displayed here as a function of q_{core}, the average value of q in the region $0.0<\hat{\rho}<0.3$. The total plasma current was varied at constant toroidal field in order to change the value of q_{95}, a reactor-relevant optimization method since fusion gain Q increases strongly with B.

Two separate sets of discharges were studied. In the first set, β_N was held approximately constant at 2.7–2.8 through feedback control of the neutral beam power (with 8–10 MW required). In the second set of discharges, the neutral beam input power was increased to the maximum available (13.5 MW) resulting in $\beta_N \approx 3.5$. Two exceptions, the highest and lowest q_{min} discharges at $q_{95} = 6.8$, achieved lower, 3.1, or higher 3.8, values of β_N respectively. The maximum β_N in the experiment was above the calculated ideal no-wall n=1 stability limit and within 5%–25% of the stability limit calculated with a perfectly conducting wall. The data presented in the figures in this report are the average of measurements obtained during the approximately constant β_N phase of each discharge and the error bars show the standard deviation. Reconstructed equilibria together with the measured temperature and density profiles were used in the ONETWO [5] code to compute from models J_{BS} [6,7], J_{NBCD} (using NUBEAM [8]) and J_{ECCD} (using TORAY-GA [9]).

The theoretical dependence of J_{BS} on the temperature, density, and q profiles is well illustrated by the form of the model [6,7]. J_{BS} is directly proportional to the local value of q and the total bootstrap current density is the sum of four terms, each proportional to the gradient of n_e, n_i, T_e, or T_i, the electron and ion densities and electron and ion temperatures, respectively.

$$\langle\langle J_{BS}B\rangle\rangle = -\frac{Fq}{B_{T0}\rho}\left[T_e\frac{\partial n_e}{\partial\rho}\mathcal{L}_{31} + n_e\frac{\partial T_e}{\partial\rho}\left(\mathcal{L}_{31}+\mathcal{L}_{32}\right) + T_i\frac{\partial n_i}{\partial\rho}\mathcal{L}_{31} + n_i\frac{\partial T_i}{\partial\rho}\left(\mathcal{L}_{31}+\alpha\mathcal{L}_{34}\right)\right] \quad . \qquad (2)$$

Here, $q = B_{T0}\,\rho\,\partial\rho/\partial\psi$ was used in Eq. (5) of Ref. [6], ψ is the poloidal magnetic flux, $F(\rho) = RB_T$, B_{T0} is B_T at a reference major radius R_0, normally the center of the vacuum vessel, $\mathcal{L}_{31}$, $\mathcal{L}_{32}$, $\mathcal{L}_{34}$, and α are functions of the trapped particle fraction and the collisionality defined in Ref. [6], and $\langle\langle\ \rangle\rangle$ indicates flux surface average. Note that because the trapped particle fraction is zero on the axis in the approximation used here, J_{BS} always drops rapidly to zero between $\hat{\rho} \approx 0.1$ and the axis.

3. Density and Temperature Profiles

The electron and ion temperatures increase across the entire profile as q_{95} decreases at constant q_{min} [Figs. 1 and 2]. This is consistent with the increase in stored energy necessary to maintain a constant value of β_N as I_p is increased at constant B_T and with the increase in τ_E with I_p.

At constant $\beta_N \approx 2.8$, the electron and ion temperature profiles broaden as q_{min} increases. This change is most clearly shown by the electron temperature profiles [Fig. 1(a)] where, at fixed q_{95}, the values at the axis and at the top of the H-mode pedestal are nearly independent of q_{min} while the values at mid-radius increase significantly as q_{min} increases. In the H-mode pedestal region ($0.8<\hat{\rho}<1.0$), $|\partial T_e/\partial\rho|$ and $|\partial T_i/\partial\rho|$ increase as q_{95} decreases, reflecting

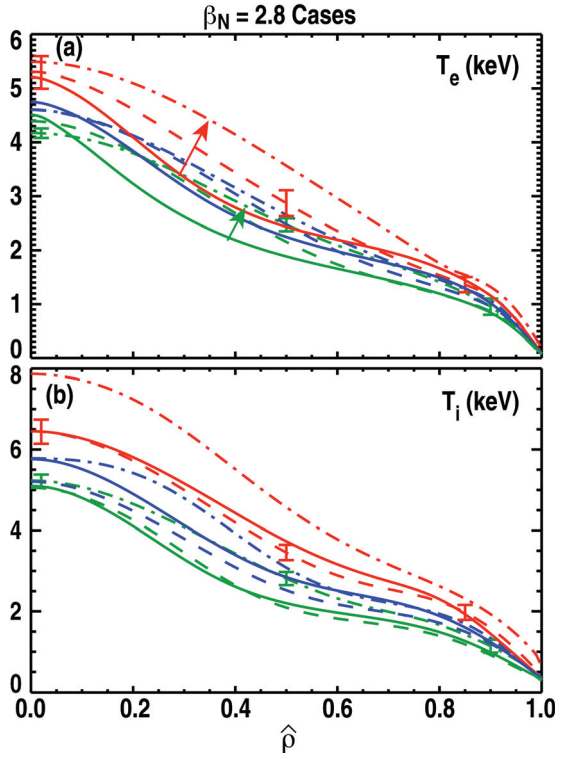

FIG. 1. For the series of discharges at β_N=2.8, (a) electron temperature and (b) ion temperature. In (a), the arrows highlight the increase in temperature at mid-radius that indicates the broadening of the profiles with increases in q_{min}. The color of the curves indicates the value of q_{95}: 4.5 (red), 5.6 (blue), 6.8 (green). The line type indicates the approximate value of q_{min}: 1.0 (solid), 1.5 (dashed), 2.0 (dot-dash).

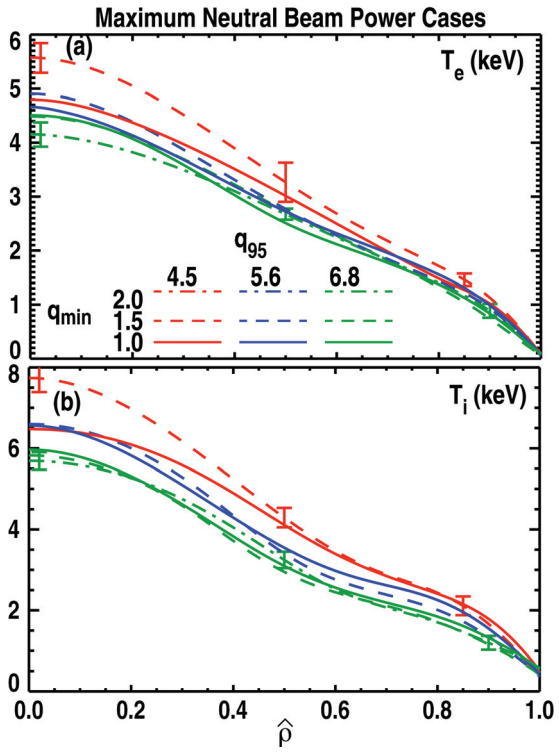

FIG. 2. For the series of discharges with the maximum available neutral beam power, (a) electron temperature and (b) ion temperature. The line types and colors are as described for Fig. 1.

an increased pedestal height, while there is no systematic trend with q_{min}.

With the maximum beam power, the temperature profiles are significantly broader in the $q_{min}\approx1$ and $q_{min}\approx1.5$ cases (Fig. 2). As a result, the temperature profiles are nearly independent of q_{min}. The exception is the case at $q_{min}\approx1$, q_{95} = 4.5 where the temperature increases with beam power were small.

The pumping of the particle exhaust in the divertor region results in relatively low pedestal density, peaked density profiles, and little systematic dependence on the q profile. At $\beta_N\approx2.8$ [Fig. 3(a)], in the region nearest the axis ($0<\hat{\rho}<0.5$), n_e is highest at the lowest values of q_{95} at a given q_{min}, but there is no consistent dependence on q_{min}. The lowest values of n_e in the pedestal are at the highest value of q_{min}, but there is otherwise no systematic dependence on the q profile. When β_N is increased to the maximum possible with the available neutral beam power, the electron density increases, most noticeably at the H-mode pedestal, and the profiles broaden [Fig. 3(b)].

The key feature in the scaling of the density and temperature profiles with the q profile is the broadening of profiles as a result of either increases in q_{core} or β_N. This is reflected in the scaling of the peaking factor for the thermal pressure

$$f_p = \left[n_e(0)T_e(0) + n_i(0)T_i(0)\right] / \left\langle n_eT_e + n_iT_i \right\rangle \quad (3)$$

as shown in Fig. 4. At $\beta_N\approx2.8$, the pressure is systematically less peaked at higher values of q_{core} and the pressure peaking is significantly reduced at the maximum achieved β_N. There is little dependence of the pressure peaking on q_{core} in the high β_N cases as all of the profiles are relatively broad.

4. Bootstrap Current Density

At $\beta_N\approx2.8$, the calculated bootstrap current density is peaked near $\hat{\rho}=0.1$ [Fig. 5(a)]. The maximum J_{BS} is in the discharges at $q_{min}\approx1$ where the peak values of $|\partial n_e/\partial\rho|$ are the largest (Fig. 3), but at mid-radius ($\hat{\rho}$ = 0.5–0.7) these discharges have a small density gradient

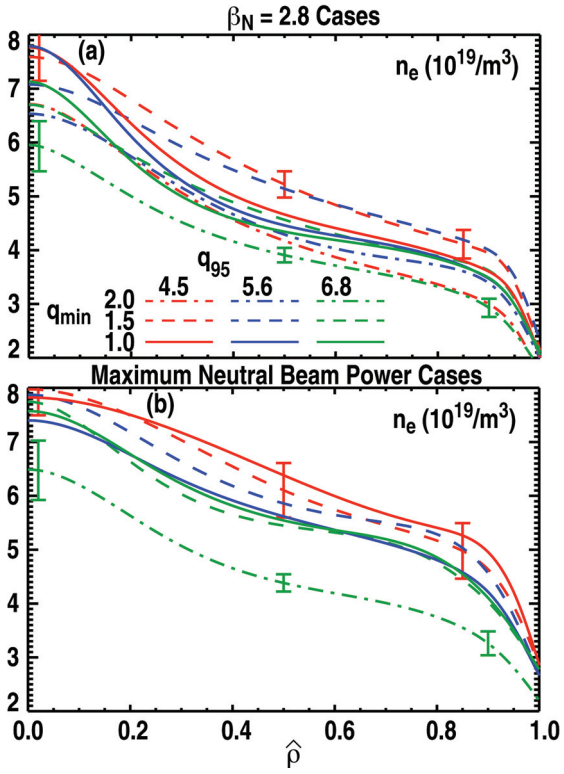

FIG. 3. Electron density for the discharges (a) at β_N=2.8 and (b) with the maximum available neutral beam power. The line types and colors are as described for Fig. 1.

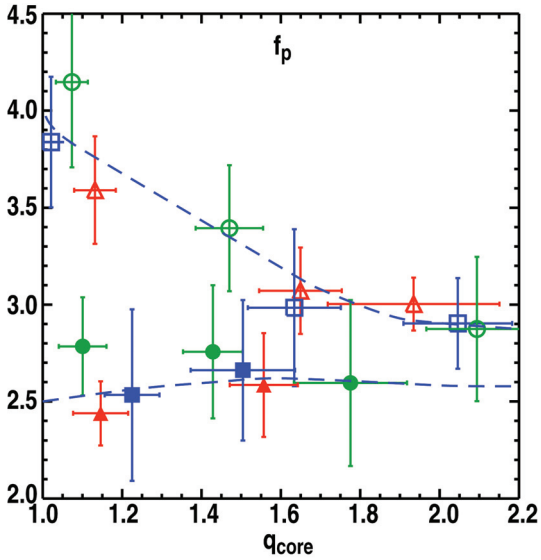

FIG. 4. The peaking factor for the thermal pressure, as defined in Eq. (3), for all of the $\beta_N\approx2.8$ (open symbols) and maximum neutral beam power (closed symbols) discharges. The dashed lines highlight the trends. The symbol types and colors indicate the value of q_{95}: 4.5 (red triangles), 5.6 (blue squares), 6.8 (green circles).

and thus the smallest J_{BS}. In most of the region $0<\hat{\rho}<0.7$, at a given q_{min}, J_{BS} is highest at the lowest value of q_{95}. In the H-mode pedestal region there is no systematic variation of J_{BS} with q_{min} or q_{95}. In this region the larger temperature gradients at lower q_{95} are compensated by the q scaling of J_{BS}.

At the β_N produced with the maximum available neutral beam power, the J_{BS} profile is significantly broader than at $\beta_N \approx 2.8$ [Fig. 5(b)]. The peak values near $\hat{\rho}=0.1–0.2$ are reduced by up to a factor of 2.5, and the bootstrap current density is increased at mid-radius. These changes are the result of broadening of both the temperature and density profiles. In the region of the H-mode pedestal, unlike in the $\beta_N \approx 2.8$ cases, there is a systematic increase of the width of the J_{BS} peak in the pedestal region with increasing q_{95} that results primarily from an increase in the width of the electron and ion density gradient profiles.

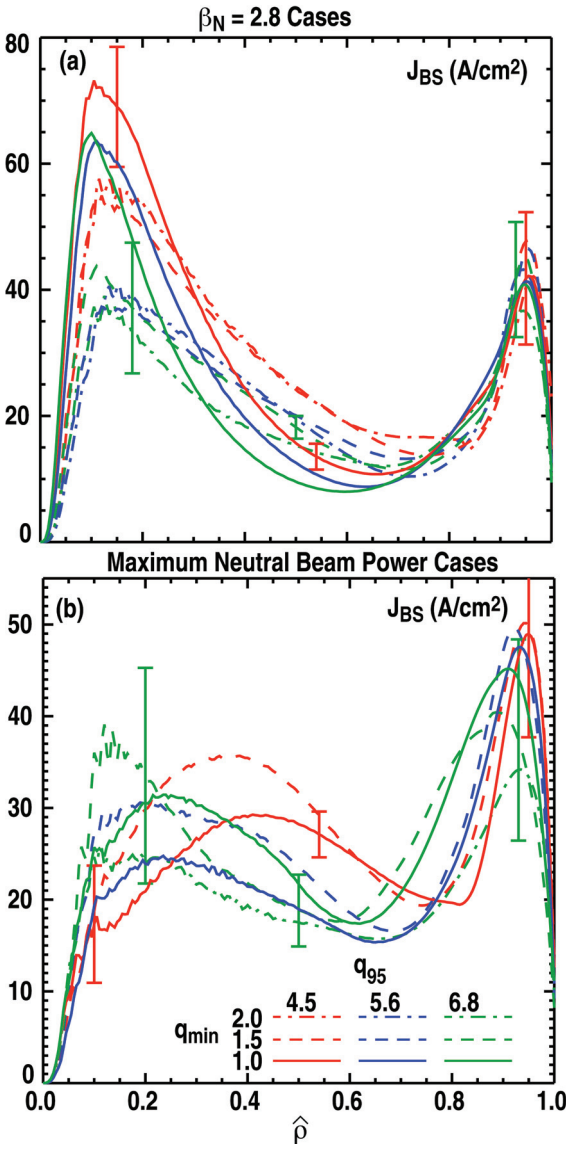

FIG. 5. Profiles of the bootstrap current density computed from Eq. (2), the measured density and temperature profiles and the reconstructed equilibria for (a) the discharges with $\beta_N \approx 2.8$, (b) the discharges heated with the maximum available neutral beam power. The line types and colors are as described for Fig. 1.

5. Scaling of f_{BS}

The calculated bootstrap current fraction for the experimental data is maximum at the largest value of q_{95} and the largest values of β_N (solid green circles, Fig. 6) in agreement with Eq. (1). A feature not included in Eq. (1), though, is that the variation of f_{BS} with q_{core} is comparable to the variation with q_{95}. At $\beta_N \approx 2.8$, the trend is for f_{BS} to increase with q_{core} with the exception of two of the data points with $q_{core} \approx 2$, where the relatively high q_{core} value is offset by broader temperature and density profiles and reduced gradients. At the maximum neutral beam power, the scaling of f_{BS} with q_{core} is similar to the scaling of β_N. For q_{95} = 4.5 and 5.6, f_{BS} increases from $q_{core} \approx 1$ to 1.5. At $q_{95}=6.8$, though, f_{BS} decreases as q_{core} increases as a result of the relatively low β_N achieved at the highest q_{core} and the relatively high β_N achieved at the lowest q_{core}.

Values of f_{BS}/β_{Nth} (Fig. 7) differ in two key ways from the proportionality to q_{95} predicted by Eq. (1). (β_{Nth} is computed from the thermal component of the pressure.) First, although the f_{BS}/β_{Nth} values scale roughly linearly with q_{95}, the data extrapolate to an offset value at $q_{95}=0$. This reflects the importance of including q_{core} in the scaling. Second, the data from the maximum beam power discharges lie systematically below the data from the $\beta_N \approx 2.8$ discharges. This reflects the broadening of the density and temperature profiles when β_N increases. The following improved scaling relation (Fig. 8) eliminates both of the

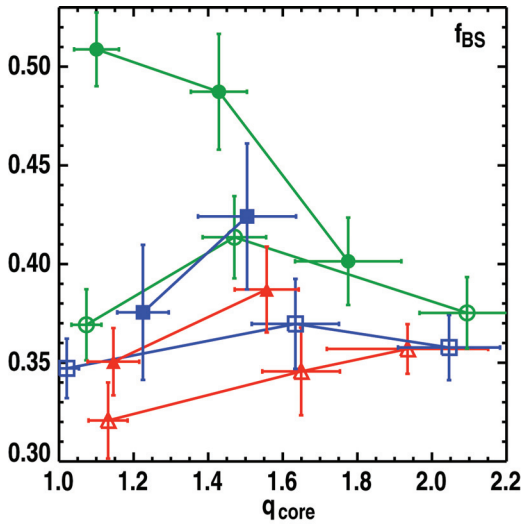

FIG. 6. Calculated fraction of the total plasma current resulting from bootstrap current (f_{BS}) for discharges with β_N=2.8 (open symbols) and discharges heated by the maximum available neutral beam power in order to maximize β_N (closed symbols). The lines connect points with the same value of q_{95}: 4.5 (red triangles), 5.6 (blue squares), 6.8 (green circles).

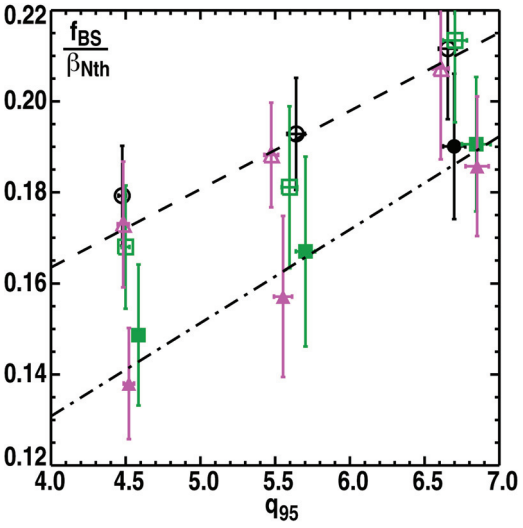

FIG. 7. Ratio of the bootstrap current fraction to the normalized beta computed from the thermal component of the pressure [Eq. (3)]. q_{core}: 1 (magenta triangles), 1.5 (green squares), ≈2 (black circles). Open symbols are for discharges with β_N≈2.8 and closed symbols are for discharges with the maximum neutral beam power.

discrepancies with Eq. (1) by including both $q_{\rm core}$ and q_{95} and by including the thermal pressure peaking factor [Eq. (3)] to account for changes in the shape of the temperature and density profiles.

$$f_{\rm BS}/\beta_{\rm Nth} = Aq_{\rm core}f_{\rm p}^{\alpha_{\rm core}} + Bq_{95}f_{\rm p}^{\alpha_{95}} \qquad (4)$$

In this function, the total bootstrap current is separated into a component in the innermost portion of the discharge that scales with $q_{\rm core}$ and a component in the outermost portion that scales with q_{95}. There are separate exponents with opposite signs on the thermal pressure peaking factor for the two terms ($\alpha_{\rm core}$≈3.0, α_{95}≈-0.94) because, as $f_{\rm p}$ varies, the gradients in the innermost and outermost portions of the discharge change in opposite directions and at different rates.

6. Total Noninductively Driven Current

In almost all cases, the calculated $f_{\rm NI}$ increases with both $q_{\rm core}$ and q_{95} (Fig. 9) as a result of the combined changes in $f_{\rm BS}$ (Fig. 6) and $f_{\rm NBCD}$. Electron cyclotron current drive provided only 2%–4% of the total current because of the relatively high electron density.

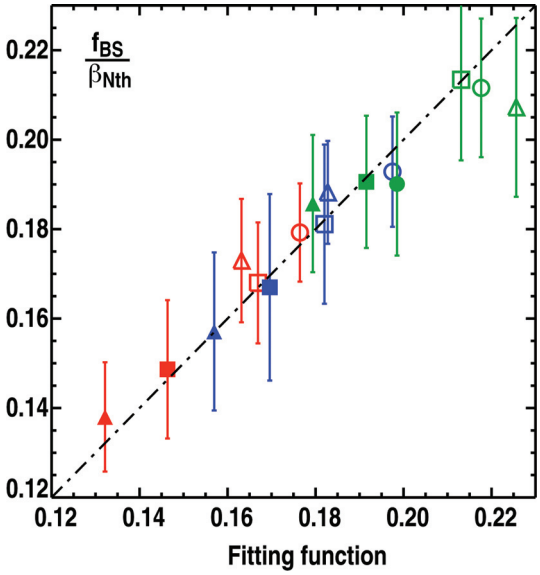

FIG. 8. A fit of f_{BS}/β_{Nth} to the function specified in Eq. (4). The values computed from the experimental data are plotted versus the values computed from the fitting function with A = 0.0018±0.0015, B = 0.052±0.045, α_{core}= 3.0±0.75, and α_{95}=-0.94±0.94. Open symbols are discharges with β_N≈2.8 and closed symbols are discharges with the maximum neutral beam power. The colors indicate the value of q_{95}: 4.5 (red), 5.6 (blue), 6.8 (green). The symbol shapes represent the nominal value of q_{core}: 1 (triangles), 1.5 (squares), ≈2 (circles).

f_{NBCD} increases with q_{core}, a result of higher T_e and reduced n_e, and increases with q_{95}. The sole exception to the increase in f_{NI} with q_{core} is the maximum neutral beam power discharge at $q_{core}\approx1.77$, $q_{95}=6.8$ where f_{NI} is similar to the value in lower q_{core} discharges as a result of relatively low β_N and therefore relatively low f_{BS}.

Comparison of the calculated J_{NI} to J identifies the q profiles that can best be maintained with noninductively driven current and thus are best suited to steady-state operation. The optimum q profile is one with a high fraction of bootstrap driven current and a good match between the shape of the residual current density profile ($J - J_{BS}$) and the known methods to efficiently drive current by external means.

The highest bootstrap current fraction was found at the highest β_N, the highest $q_{95}=6.8$ and $q_{core}\leq1.5$. However, in the highest β_N discharges, in the region between the axis and the H-mode pedestal the J_{BS} profiles are relatively uniform. In contrast, the profiles of J peak near the axis (Fig. 10). Current driven by neutral beams injected at the discharge midplane provided most of the externally driven current needed to match J - J_{BS} because the J_{NBCD} profile is peaked near the axis and rather broad. The match between J_{NI} and J in the region $\hat{\rho}<0.2$ varies strongly with q_{core}. At $q_{core}\approx1.1$ [Fig. 10(a)] the residual current density is very large in this region because J is large and because relatively high n_e resulted in a relatively low peak value of J_{NBCD}. At $q_{core}\approx1.77$ [Fig. 10(c)], J_{NI} exceeds J near the axis because the neutral beam driven current is the largest at this q profile and J is reduced at higher q_{core}. Noninductive current overdrive near the axis ($J_{NI}>J$) will reduce q_{core} in steady state.

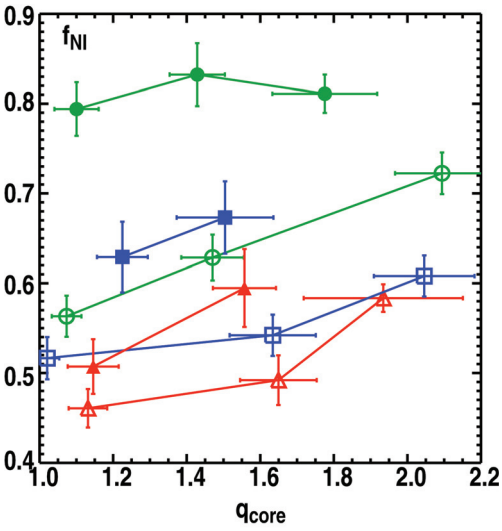

FIG. 9. The computed noninductive current fraction. The open symbols are for the discharges with $\beta_N\approx2.8$ and the solid symbols are for the discharges heated by the maximum available neutral beam power. The lines connect data points with the same value of q_{95}: 4.5 (red triangles), 5.6 (blue squares), 6.8 (green circles).

7. Summary

Systematic changes in the shapes of the density and temperature profiles were found as q_{min} and q_{95} were varied over the range of interest for tokamak operation with 100% of the current driven noninductively. There were also systematic changes as β_N was varied. The primary change was a broadening of the profiles as either q_{core} or β_N was increased. The broadening of the density and temperature profiles reduces the gradients and, as a result, J_{BS}. Thus the J_{BS} profiles are peaked near $\hat{\rho}\approx0.1$ at $\beta_N\approx2.8$, but are much more uniform in the region inside the H-mode pedestal at the highest values of β_N. In addition, the highest values of f_{BS} are at the mid-range value of q_{core}. Equation (1) is not a good predictor of f_{BS} over the range of parameters of the discharges in this experiment. A scaling function of the form in Eq. (4) provides a much more complete description.

The relatively uniform J_{BS} profiles in the region inside the H-mode pedestal in the highest β_N discharges are not a good match to the peaked profile of J in the weak shear discharges produced for this experiment. In addition, J_{BS} is only a small fraction of J in the innermost portion of the discharge (e.g. $\hat{\rho}<0.5$). Therefore, externally driven noninductive current must be provided with a peaked profile so that J_{NI} is sufficiently peaked.

Of the discharges produced for this experiment, the three with q_{95}=6.8 are reasonable candidates for reproducible f_{NI}=1 operation in DIII-D with the present, or soon to be available, external current drive capability. Two of the three discharges had f_{BS}≈0.5 and all three had f_{NI}≈0.8. In the two discharges with $q_{core} \geq 1.43$, in order to increase f_{NI} to 1, additional external current drive of ≈20 A cm^2 is required in the region $0.2<\hat{\rho}<0.7$. This additional current drive could be provided by the DIII-D ECCD system or by the planned off-axis neutral beam injection [10]. In the discharge with q_{core}≈1.1, the total additional externally driven current that is needed is the same as in the two higher q_{core} discharges, but the required current density is 2 to 3 times higher and it must be located near the axis. As ECCD is more efficient on axis than off axis, this required noninductive current could also be provided by the DIII-D ECCD system [11].

This work was supported in part by the US Department of Energy under DE-FC02-04ER54698, DE-AC52-07NA27344, DE-AC05-06OR23100, DE-FG02-08ER54984, and DE-AC05-00OR22725.

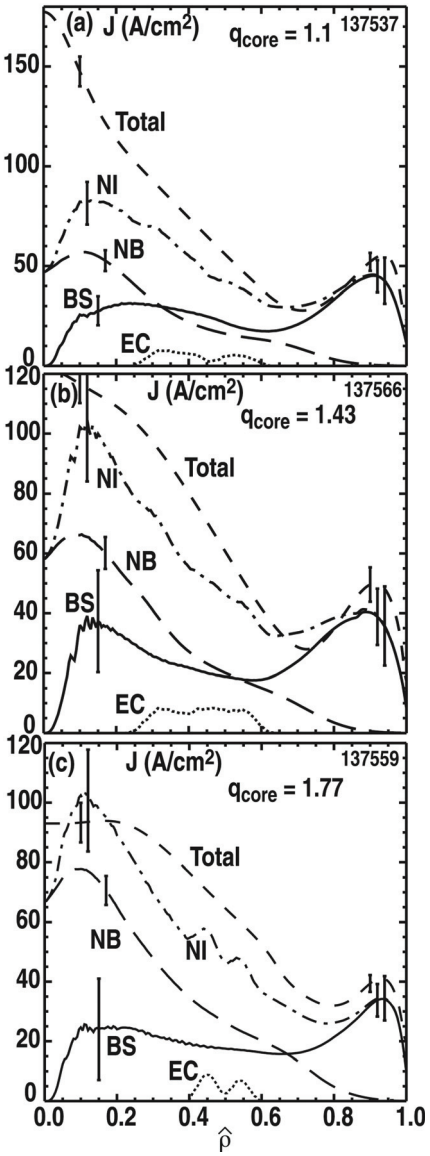

FIG. 10. Radial profiles of current density in discharges with maximum available neutral beam power, q_{95}=6.8 and different values of q_{core}: (a) 1.1, (b) 1.43, (c) 1.77. The total current density (dashed line) is taken from the equilibrium reconstruction, the bootstrap current density (solid line), neutral beam driven current density (long dashed line) and electron cyclotron driven current density (dotted line) are calculated from models. The total noninductive current density (dash-dot line) is $J_{NBCD} + J_{ECCD} + J_{BS}$.

References

[1] BICKERTON, R.J., et al., Nature Physical Science **229** (1971) 110.
[2] LUCE, T.C., "Realizing steady-state tokamak operation for fusion energy," submitted to Phys. Plasmas (2010).
[3] GORMEZANO, C., et al., Nucl. Fusion **47** (2007) S285.
[4] HOLCOMB, C.T., et al., Phys. Plasmas **16** (2009) 056116
[5] ST JOHN, H.E., et al., Proc. 15th Int. Conf. on Plasma Phys. and Control. Nucl. Research, Vol. 3, Seville, 1994 (IAEA, Vienna, 1995) p. 603
[6] SAUTER, O., et al., Phys. Plasmas **6** (1999) 2834
[7] SAUTER, O., et al., Phys. Plasmas **9** (2002) 5140
[8] PANKIN, A., et al., Comput. Phys. Commun. **159** (2004) 157
[9] LIN LIU, Y.R., et al., Phys. Plasmas **10** (2003) 4064
[10] MURAKAMI, M., et al., Nucl. Fusion **49** (2009) 065031
[11] PETTY, C.C., et al., Bull. Am. Phys. Soc. **54** (2009) 166